

*Biochemistry.* Author manuscript; available in PMC 2013 August 14.

Published in final edited form as:

Biochemistry. 2012 August 14; 51(32): 6432-6440. doi:10.1021/bi300733d.

# Nanoscale structure and dynamics of ABOBEC3G complexes with single-stranded DNA

Luda S. Shlyakhtenko<sup>1</sup>, Alexander Y. Lushnikov<sup>1</sup>, Atsushi Miyagi<sup>1</sup>, Ming Li<sup>2</sup>, Reuben S. Harris<sup>2</sup>, and Yuri L. Lyubchenko<sup>1,\*</sup>

<sup>1</sup>Department of Pharmaceutical Sciences, College of Pharmacy, University of Nebraska Medical Center: 986025 Nebraska Medical Center. Omaha. NE 68198-6025

<sup>2</sup>Department of Biochemistry, Molecular Biology, and Biophysics, Institute for Molecular Virology, Center for Genome Engineering, Masonic Cancer Center, University of Minnesota, 321 Church Street S.E., 6-155 Jackson Hall, Minneapolis, MN 55455

#### **Abstract**

The DNA cytosine deaminase APOBEC3G (A3G) is capable of blocking retrovirus replication by editing viral cDNA and impairing reverse transcription. However, the biophysical details of this host-pathogen interaction are unclear. Here we applied atomic force microscopy (AFM) and hybrid DNA substrates to investigate properties of A3G bound to single-stranded DNA (ssDNA). Hybrid DNA substrates included ssDNA with 5' or 3' ends attached to DNA duplexes (tail-DNA) and gap-DNA substrates, in which ssDNA is flanked by two double-stranded fragments. We found that A3G binds with similar efficiency to the 5' and 3' substrates, suggesting that ssDNA polarity is not an important factor. Additionally, we observed that A3G binds the single-stranded region of the gap-DNA substrates with the same efficiency as tail-DNA. These results demonstrate that single-stranded DNA ends are not needed for A3G binding. The protein stoichiometry does not depend on the ssDNA substrate type, but the ssDNA length modulates the stoichiometry of A3G in the complex. We applied single molecule high-speed AFM to directly visualize the dynamics of A3G in the complexes. We were able to visualize A3G sliding and protein association-dissociation events. During sliding, A3G translocated over a 69 nucleotide ssDNA segment in less than 1 second. Association-dissociation events were more complex, as dimeric A3G could dissociate from the template as a whole, or undergo a two-step process with monomers capable of sequential dissociation. We conclude that A3G monomers, dimers, and higher order oligomers can bind ssDNA substrates independent of strand polarity and availability of free ssDNA ends.

#### **Keywords**

APOBEC3G; single-stranded DNA binding proteins; site search mechanisms; atomic force microscopy; AFM; high speed-AFM

The human APOBEC3G (A3G) protein belongs to a family of DNA cytosine deaminases (1, 2). Several of these proteins, including A3G, have the capacity to block HIV-1 replication

Corresponding author: Yuri L. Lyubchenko, Department of Pharmaceutical Sciences, College of Pharmacy, COP 1012, University of Nebraska Medical Center, 986025 Nebraska Medical Center, Omaha, NE 68198-6025, 402-559-1971 (office), 402-559-9543 (fax), ylyubchenko@unmc.edu.

Supporting Information

Additional information for the Methods section, schematics explaining the design of the DNA substrate, AFM images of A3G-DNA complexes, graphs characterizing A3G-DNA complexes, and movies of animated time-lapse AFM images of the complexes. This material is available free of charge via the Internet at http://pubs.acs.org.

by editing viral cDNA and impairing cDNA synthesis ((3) and references therein). A3G has two domains: an N-terminal pseudo-catalytic domain (PCD) and a C-terminal catalytic domain (CD) (4–6). NMR and X-ray crystal structures have been obtained for the CD, but thus far the PCD and the full-length apo-enzyme have resisted structural interrogation (7–12).

Several genetic and biochemical studies have concluded that the CD domain alone is responsible for deamination activity (4-6, 13-15), whereas the PCD domain is more important for binding RNA or single-stranded DNA (ssDNA), mediating oligomerization, and interacting with the natural A3G antagonist HIV-1 Vif (4, 5). In spite of the seemingly different functions of the CD and PCD domains in (6), it was suggested that the PCD domain indirectly contributes to catalysis by mediating A3G scanning of ssDNA. Moreover, it was reported in (16) that the antiviral function of A3G protein cannot be attributed solely to its cytosine deaminase function. Also in (17), using point mutations to the C and N terminal active sites, it was suggested that the entire protein structure is necessary for its antiviral function. Systematic biochemical studies (5, 16, 18, 19) indicated that the deaminase reaction of A3G protein occurs predominantly in 3'-5' direction. Therefore, one asks the questions of whether the polarity of the DNA substrate is important for complex formation and how availability of free 5' or 3' ssDNA ends might affect ssDNA-protein complex formation. The requirement of the DNA binding domain for enzyme processivity and polarity was proposed in (5), but so far, no evidence supporting this model has been obtained. In this study, we address the possible roles of DNA substrate polarity and free ends in A3G-ssDNA complex formation.

Atomic force microscopy (AFM) has already been instrumental in the characterization of complexes of A3G with ssDNA, specifically in the evaluation of protein stoichiometry (5, 18, 20). The analysis of the AFM data led the authors to conclude that A3G, in complexes with ssDNA substrates, exists as dimers, tetramers and higher oligomers, defining the directional deamination reaction of the enzyme (5, 18). They also showed that cations contribute to protein oligomerization, but play a secondary role. However, the use of ssDNA substrates in these studies complicated distinguishing between complexes and free protein. Both the complexes and free proteins are morphologically similar and appear on the AFM images as round-shaped, globular features. The ambiguity issue was resolved in our recent paper (20), in which AFM was used to analyze A3G bound to a hybrid ssDNA substrate. In this approach, ssDNA (69 nucleotides) is attached to the double-stranded DNA fragment, which acts as an in-built ruler. Protein bound to such a substrate appears on the AFM images as a globular feature (blob), located at the end of the DNA duplex. This hybrid substrate enabled us to use volume measurements to determine A3G stoichiometry in both free and ssDNA-bound states. We observed that A3G protein binds ssDNA mostly as a dimer. A3G stoichiometry increased slightly with the addition of Mg<sup>2+</sup>, but dimers remained predominate form when Mg<sup>2+</sup> was depleted.

Here, we developed the hybrid DNA approach further to characterize the ssDNA binding properties of A3G. We designed 3' and 5' ssDNA ends (3' tail-DNA and 5' tail-DNA respectively), attached to the dsDNA fragments to understand whether the polarity of the single-stranded ends affects A3G binding. In addition, we designed the substrates, such that the ssDNA region is located between DNA duplexes (gap-DNA), to see how critical the ssDNA end is for A3G-complex formation. Note that DNA molecules of such types are formed during DNA replication and repair, and may be substrates for deamination by one or more A3 family members (21–23). Additionally, we made tail-DNA substrates with different lengths to answer the question of whether the length of the ssDNA contributes to A3G oligomerization. Using high speed-AFM (HS-AFM) we analyzed dynamics of A3G in complexes with these hybrid DNAs. These studies indicate that both A3G monomers and

dimers form stable complexes with ssDNA. We also directly observed dissociation-association events for A3G suggesting that this protein utilizes a three dimensional mechanism for the site search. Additionally, we visualized one-dimensional movement of A3G over ssDNA substrates. These findings suggest how A3G might engage ssDNA substrates inside retrovirus cores during reverse transcription.

# **Material and Methods**

# **APOBEC3G** preparation

Details for preparing human A3G-myc-His have been reported (12, 20). A representative gel image and activity data are shown in Figure S5 (Supporting Information, SI).

# Preparation of hybrid DNA substrates

Preparation of the hybrid dsDNA with single-stranded tails: tail-DNA—To construct the dsDNA with single-stranded tails attached (tail-DNA), we followed the procedures described in detail in (20, 24). Figure S1 (SI) shows the schematic for preparation of tail-DNA. First, the PCR product digested with restriction enzyme was extracted and purified from agarose gels. Second, the synthetic oligonucleotide annealed with the adapter, was ligated with the restriction fragment. Third, the ligated mixture was separated on an agarose gel, extracted and purified using the Qiagen gel extraction kit. The final product was re-suspended in 10 mM Tris-HCl, pH 7.4, 1 mM EDTA (TE buffer). The conditions for the annealing and ligation procedures are described in detail in the Supporting information and Methods sections SM1 and SM2 and the sequences are summarized in Table ST1 (SI).

**Preparation of hybrid DNA with a single-stranded region in the middle: gap-DNA**—Figure S2 shows the schematic for the preparation of hybrid dsDNA with a single-stranded DNA region in the middle. First, the two 5' and 3' tail-DNAs were mixed in a 1:1

stranded DNA region in the middle. First, the two 5' and 3' tail-DNAs were mixed in a 1:1 ratio and annealed with the bridge oligos (see mixing- annealing steps). Then, the annealed product was ligated overnight at 16 °C. To remove the bridge-oligos, the product after ligation was heated up to 70 °C for 5 min and immediately put into ice. The final product, separated from the bridge-oligos in an agarose gel, was extracted, purified and re-suspended in TE buffer. The detailed conditions for obtaining hybrid gap-DNA are described in the Supporting information and Methods section SM3 and all sequences are provided in SI Table ST2.

#### Preparation of A3G-DNA complexes

A3G was mixed with different DNA substrates at a 5:1 protein/DNA molar ratio in a reaction buffer containing 50 mM HEPES, pH 7.5, 100 mM NaCl, 5 mM Mg<sup>2+</sup> and 1 mM DTT, incubated at 37 °C for 10 min followed by purification using a Montage UFC spin-column, as described in detail in (20).

# Sample preparation and AFM imaging of dry samples

For AFM sample preparation, the 1-(3-aminopropyl)silatrane (APS) functionalized mica was used as described in (24, 25). 5  $\mu$ L of sample was deposited on APS mica for 2 min, rinsed with deionized water and dried with Ar gas. Images were acquired in tapping mode in air using the Multimode Nanoscope IV system Bruker, (Santa Barbara, CA). Silicon probes with 42N/m at resonance frequencies between 310–340 kHz were used.

# **High-Speed AFM in liquid**

The mica (1.5 mm  $\times$  1.5 mm) was glued to a glass cylinder attached to the AFM scanner, cleaved, and treated with an APS solution as described above. A drop of the A3G-hybrid DNA complex (2  $\mu L$ ), prepared as described in the section on preparation of A3G-hybrid DNA complexes, was deposited on the mica surface for 5 min. The scanner with the sample was immersed in 200  $\mu L$  of a buffer solution. All images were taken in the buffer without drying the sample.

The HS-AFM images were acquired by using the HS-AFM instrument developed in the Ando group (Kanazawa University, Kanazawa, Japan, and distributed by RIBM Co. Tsukuba, Japan) (26). The data were acquired by operating the instrument in tapping mode in liquid. Silicon nitride AFM probes (BLAC10EGS, Olympus) were etched using the electron beam deposition (EBD) procedure. The spring constant of the AFM probes was between 0.1 and 0.2 N/m, with the resonance frequency between 400 and 1000 kHz in water. Continued scanning over the selected area (200 nm  $\times$  200 nm) was performed to follow the dynamics of A3G-DNA complexes. The scan rate varied between 720 and 990 ms/frame.

### Data analysis

For each protein-ssDNA complex, we measured the length of each double-stranded hybrid DNA arm. Proteins volumes were calculated from measured AFM image heights and diameters using cross-section option in Femtoscan Online (Advanced Technologies Center, Moscow, Russia) similar to the procedure described earlier (20). The conversion coefficient, as described in (20, 27, 28), calculated from the dependence of the protein volume on the molecular weight (Fig. S6; SI) was used to calculate the stoichiometry of proteins within complexes. To minimize unavoidable tip convolution effect, the heights and widths of DNA duplexes were measured on the same images and the data with similar DNA parameters were used for the volume measurements. The data for measurements of protein volume and length of DNA arms were summarized into histograms using Origin 6.0 (Originlab, Northampton, MA).

# Results

#### 1. A3G binds equivalently to 5' and 3'-ending ssDNAs

A3G, as a retroviral ssDNA deaminase, appears to have 3′-5′ polarity (5). Therefore, we first sought to address the question of whether polarity affects A3G binding to ssDNA, by testing complex formation between A3G and two 69nt long tail-DNA substrates with 5′-end and 3′-end polarities. Due to the differences in lengths of the dsDNA arms attached to the 69ss tail-DNA (3′-69ss-436bp and 5′-69ss-231bp), these different substrates could be visualized with AFM at the same image. The use of the 1:1 mixture of both DNA substrates eliminates potential concerns with the variability of conditions if the complexes are prepared with each substrate separately. Fig. 1A shows a typical AFM image obtained for such a mixture. In this image, the complexes with 5′-tail-DNA are marked with (1) and 3′-tail-DNA complexes are marked with (2). Complexes formed with similar yields, 88% for A3G complexed with 5′-69-tail-DNA and 87% for A3G complexed with 3′-69ss tail-DNA. Similar designs with shorter lengths of ssDNA were made and the yields were 70% for 5′-42ss tail-DNA, 63% for 3′-42ss tail-DNA, 34% for 5′-27 tail-DNA and 35% for 3′-27ss tail-DNA, indicating that the polarity of the single-stranded regions has no effect on efficiency of complex formation.

To determine the stoichiometry of the complexes formed between A3G and 3' and 5' tail-DNA, we calculated the volume of the protein in the complex. The volume distribution of

complexes compiled from the analysis of more than 150 molecules is shown in Figs. 1. B, C. The distributions for 3'-69ss and 5'-69ss tail-DNA are similar, with the maxima on both distributions at approximately 120 nm<sup>3</sup>. According to the conversion coefficient determined previously (20), this value corresponds to A3G dimers. Similar to our previous work (20), monomers, trimers and tetramers are also present in each distribution, but the majority of the A3G-ssDNA complexes correspond to dimers.

## 2. A3G binds equivalently to terminal and internal ssDNA regions

To understand whether the single-stranded end of the DNA is required for complex formation and if an internal ssDNA region might also bind to A3G, we designed a substrate with a 69 nt long ssDNA region flanked by double stranded DNA arms (69ss gap-DNA substrate). A3G complexes with this substrate were prepared in parallel with the 69ss tail-DNA substrate and imaged using AFM. Typical images for complexes made with the 69ss tail-DNA and 69ss gap-DNA substrates are shown in Figs. 2A and 2B, respectively. A3G binds the substrate at the end of 69ss tail-DNA (plate A) or inside of the 69ss gap-DNA substrate (Plate B). Galleries of more AFM images for complexes of A3G with tail-DNA and gap-DNA are shown in Figs. 2C and 2D, respectively. The bright protein blobs representing complexes of A3G and gap-DNA are located approximately one-third the distance from the closest end. The length measurements confirmed that the position of A3G protein corresponds to the location of the single-stranded region within the gap-DNA. We also measured the yields of complexes in these two preparations. They were 50% and 40% for A3G complexes with the tail-DNA and gap-DNA, respectively, suggesting that the end of the single-stranded region is not essential for complex formation.

There is some variability in A3G complex sizes in the AFM image gallery. We measured the protein volumes in multiple images to estimate A3G stoichiometry, as performed in (20). Based on these measurements, in Fig. 2A we marked dimers as 2 and trimers as 3. Similar heterogeneity in the protein sizes was observed for the complexes with the gap-DNA substrate (Fig. 2B). In this figure complex as a dimer is marked as 2 and monomer 1. The protein stoichiometry determined from the volume measurements for the gap-DNA and tail-DNA complexes are shown in Figs. 3A and B, respectively. The histograms for tail-DNA and gap-DNA are very close with the maxima on both distributions, at approximately 120 nm³, which corresponds to an A3G dimer (indicated with an arrow in Fig. 3A, B). A3G monomers, and higher order multimers are also present in the distributions.

# 3. Dependence of A3G mode of binding on the length of ssDNA

To determine the effect of ssDNA length on A3G protein oligomerization, we examined A3G protein in complexes with 42nt, 27nt and 18nt tail-DNA. The data for the protein volume distribution for the A3G complexes with 27nt are shown in Fig. 4. Similar to longer tails, the histogram for 27ss tail-DNA complexes with A3G has the maximum distribution around dimers with traces of tetramers present. Similar observations were obtained for A3G complexes with 42ss tail-DNA (see Figs. S3A, B in SI).

However, the A3G volume distribution for 18ss tail-DNA complexes was different with higher frequencies of monomers: the amount of monomers was approximately equal to the amount of dimers (shown with yellow arrows in Figs. 5A, B). Moreover, there was a decrease in the number of higher order oligomeric structures in the complex. These data clearly indicated that for short ssDNA substrates, such as 18ss tail-DNA substrates, the size of the A3G complexes was smaller with a tendency toward monomers binding. Notably, the yield of complexes also depended on the ssDNA length, with the efficiency of complex formation decreasing ~ 3 times for the 18ss-tail-DNA compared to the longer 69ss tail-DNA hybrid substrate.

# 4. Dynamics of A3G-ssDNA complexes in solution: HS-AFM data

One step and two-step protein dissociation pathways—To follow directly the dynamics of the A3G-ssDNA complexes we applied HS-AFM, which provides high resolution time-lapse images of fully hydrated biological samples in millisecond time scale (reviewed in (26, 29, 30)) including protein-DNA complexes (e.g., (31, 32)). A3G complexes with both tail-DNA and gap-DNA substrates were analyzed with HS-AFM.

We first analyzed the dynamics of A3G bound to 69ss gap-DNA substrates (Fig. 6 shows key frames from Movie 1 in Supporting information). A3G in frame 118 appears located at ~1/3 of one end of the DNA and this position corresponds to the position of ssDNA within the hybrid substrate. The short DNA arm changed shape in frame 131, but the protein remained bound regardless of the DNA segmental mobility. A3G then dissociated in one-step in frame 146. The protein volume measurements were performed for each frame of the movie dataset, and volume measurements are consistent with most substrates being bound by a dimeric form of A3G.

The dynamics of the end-bound complexes are illustrated in Fig. 7 (Movie S2 in SI). The complex shown in frame 178 dissociates after less than 10 frames (frame 187), but due to the DNA dynamics it forms again (frame 196) and remains bound for a long time (almost 200 frames; frame 391) regardless of the ongoing DNA movement. Interestingly, the dissociation of the complex and its assembly after approaching the DNA occurs fast, during the acquisition of one frame. According to the volume measurements, these dynamics mostly represent the dimeric form of A3G.

Previous results illustrated that A3G dimers can dissociate from and reassociate with ssDNA substrates. However, each protein monomer contains a ssDNA-binding domain, so theoretically each A3G monomer alone should be capable of intrinsically binding to ssDNA. HS-AFM was instrumental in identifying of both binding modes. Figure 8 and Movie S3 demonstrate the dynamics of A3G bound to a 69ss tail-DNA substrate (Movie S3, SI). Frame 310 shows an A3G dimer bound to ssDNA. Frame 318 shows that indeed the protein dissociates into two blobs with one going away and another remaining bound to the same substrate. The protein remains bound (frame 323) and later dissociates from the substrate (frame 404) and goes away from the observation area. Volume measurements are consistent with the dissociated protein being an A3G monomer. This process was termed two-step dissociation.

**A3G** one-dimensional movement—Next we analyzed the dynamics of A3G bound to ssDNA substrates. It was proposed in (16, 33) that A3G utilizes various mechanisms including one-dimensional diffusion or sliding. The high temporal resolution of HS-AFM is sufficient for testing the sliding model. Frame 120 in Fig. 9A shows a complex with the A3G monomer occupying the ssDNA gap in the hybrid DNA substrate. The protein shifts its position rather shortly (frame 122) and soon moves to the right overshooting the original position (frame 153) followed by dissociation (frame 158; see Movie S4 in SI). To characterize this process quantitatively, we measured the contour lengths of the left and right DNA flanks (from the DNA end to the middle of the protein blob). The graphs (pink and green lines) show that both arms do not change the length until frame 120 (frame 120 indicated by arrow on the graph). Between frames 120 and 122 left arm (pink line and squares) decreases by ~ 20 nm, whereas the right arm (green triangles and line) increases by the same value. Interestingly, the overall contour length of the DNA molecule measured from left to right end (blue line and diamonds) remains constant during entire observation period including the time interval between frames 120 and 122. This suggests that the change of the arm's length is due to the protein sliding over the ssDNA without measurable change in ssDNA length. We estimated the protein sliding range by measuring the

displacement of the protein center to avoid the contribution of the tip convolution effect. According to the length measurements, A3G can slide over 30 nm and this range is consistent with the 69 nt length of the ssDNA segment.

Another translocation event for a tail-DNA substrate is depicted in Fig. 10A (Movie S5 in SI). Frame 78 shows two end-bound complexes with rather stable complex "a" and dynamic complex "b". As it is seen from frame 79, the protein dissociates from the ssDNA (complex "b"), but remains in a close proximity to the end. Moreover, over time, the distance between protein and ssDNA changes, getting shorter (frame 99), and disappearing in frame 121. Shortly after that the protein fully dissociates and moves far from the DNA (frame 122). We measured the contour length along the ssDNA substrate up to the center of the protein and the time-dependence distance is shown in Fig. 10B. The graph shows that the protein moves away after frame 78, but remained tethered to ssDNA during a long period of time. The average distance between protein and DNA substrate is ~20 nm that is close to almost fully extended 27 nt single stranded region. The volume measurements show that A3G protein as a monomer in complex "b" and a dimer in complex "a".

# **Discussion**

Using a hybrid DNA approach, we have demonstrated that A3G binds 5′- and 3′-terminated ssDNA substrates with similar efficiency. These findings indicate that the polarity of the ssDNA substrate is not important for A3G binding. Additionally, using gap-DNA substrates we have shown that the single-stranded DNA ends are dispensable for A3G binding, as the complexes between A3G and gap-DNA are formed with the same efficiency as complexes between A3G and the substrates containing 5′ or 3′ tail-DNA. Our data also show that at chosen conditions, namely concentration of A3G in the reaction, dimeric A3G is the predominant form binding to ssDNA. The contribution of monomers and higher order oligomers clearly depends on the lengths of the DNA substrates: the shorter the ssDNA region the lower the fraction of higher-order oligomers.

A3G has two functionally distinct subunits – a C-terminal catalytic domain (CD) and an N-terminal pseudo-catalytic domain (PCD). The latter is more positively charged at physiological conditions and is thought to function as the substrate-binding domain. It has been shown in (5, 16, 18) that A3G catalyzes deamination on ssDNA with a 3′->5′ polarity, and it was further hypothesized in (5), that A3G binding should have the same polarity. Our data do not support this hypothesis. The DNA substrates with free 3′ and 5′ ends form complexes with similar efficiency. Experiments with the length of ssDNA, which varied between 69 and 18 nucleotides, did not reveal any preferences to the polarity of ssDNA ends. Notably, in (16) the sequences of all ssDNA in the hybrid substrates contained a 5′-AAA-CCC-AAA-3′ motif that supports maximal A3G deaminase activity. Therefore, if the DNA binding and deamination properties of A3G are synchronized, the polarity effect should be highest for these sequences.

According to the model suggested in (5), monomeric A3G can have two orientations relative to the preferred 5'-CCC-3' substrate sequence and only one orientation provides the active complex. To reconcile the strong polarity effect of the deaminase activity of A3G with the lack of such directionality for binding to the DNA substrate, we propose a dynamic model in which the protein flips between the two orientations, performing deamination when it adopts the active orientation. This model is consistent with the reported processive deamination activity of A3G (5, 16, 18).

We also showed that A3G does not need ssDNA ends for complex formation. A3G binds with the same efficiency to DNA substrates without ends (gap-DNA) as compared to the

tail-DNA substrates. For all designs, no binding to duplexes DNA regions was observed. Overall these findings demonstrate a very high specificity of A3G to the ssDNA, concordant with prior studies (20, 34–37). A major difference between ssDNA and dsDNA is flexibility. The high flexibility of ssDNA substrates may facilitate swapping between the active and non-active orientations of A3G by transient dissociation-association events.

Our time-lapse HS-AFM data have provided additional insights into A3G dynamics. A3G spontaneously dissociates from ssDNA suggesting that the protein-DNA complex is quite dynamic. We did not observe stronger stability of complexes formed by A3G dimers compared to the monomers suggesting that dimerization is not required for complex stability. The dimer can dissociate from the DNA as a whole (one-step dissociation pathway) or sequentially in which each monomer can dissociate independently (two-step dissociation pathway). Notably, the remaining monomer can occupy the binding site for a long time, suggesting that the A3G monomer-ssDNA complex may be stable. These observations lead us to conclude that A3G oligomers do not increase the stability of the A3G-DNA complex, and therefore should not be favored in models for biological activity.

It was proposed that, similar to other site-specific DNA binding proteins, A3G utilizes various pathways for the recognition of the deamination sites (16, 33). Time-lapse images enabled direct observations of jumping (3D diffusion) and sliding (one-dimensional diffusion). Although A3G dissociation events discussed above are in favor of the 3D model for the site search mechanism, the ability to directly visualize the association step provides the justification for the 3D search pathway. The dissociation-association steps were directly observed in Fig. 7 in which the protein after the dissociation returned to the same site (terminal ssDNA). Importantly, the reassembled complex was very stable and did not dissociate until the end of the observation period regardless of a long-range mobility of the DNA tag. Notably, the entire dissociation-association process was observed for the protein and DNA molecules moving nearby the mica surface, so their interaction with the surface did not prevent the site recognition process and the formation of the specific complex. We used a functionalized APS-mica to reliably visualize DNA (25, 31), and along with recent HS-AFM visualization of the enzymatic cleavage of DNA (38), these observations provide additional credibility to the APS-mica methodology as a technique for the AFM visualization of protein-DNA complexes.

We were able to observe A3G sliding over ssDNA substrates. One of these observations is illustrated in Fig. 9 in which A3G translocates without dissociation over the ssDNA region of the gap-substrate. The translocation process is fast: the protein moves from one side of ssDNA to another during one scan frame, i.e. less than 1 s. Another example of the sliding process is shown in Fig. 10 in which the protein slides over a terminal ssDNA segment. After the initial quick jump (~ 1s), A3G moves with small steps. The initial jump cover almost entire ssDNA region, so the protein binds to the very end of the DNA suggesting that few nucleotide may be sufficient for A3G binding. However, compared to the gap substrates the analysis of the images with tail-substrates is more complicated. Due to a low contrast of ssDNA on the AFM images, we unable to distinguish protein sliding from the change of the length of ssDNA bound by the protein. Therefore the observed change can be due to A3G sliding as well as to changes in length of bound ssDNA. These data are consistent with A3G sliding events observed recently in a single molecule FRET study (39).

We also assessed how varying the length of the ssDNA substrate affected A3G binding and oligomerization. Results shown in Figs. 3–5 demonstrate that the major binding mode at the chosen conditions is the dimeric form of A3G, but monomers and higher oligomers are found as well. The presence of larger oligomeric A3G forms is the highest for the 69 nt long substrate, decreasing to a very small percentage for the 27 nt substrate. In the shortest 18 nt

substrate, monomers and dimers were present in equal amounts (Fig. 5), with no detectable tetramers. Oligomerization of A3G is considered a major factor in defining A3G deamination activity, and oligomers as large as tetramers are considered active forms of the protein, while dimers have appeared associated with little activity (19). In the framework of that paper, we suggest that even for the 69 nt ssDNA in which the dimers are the predominant A3G forms, only a small percentage of the complexes are active. At the same time, very few tetramers are found associated with the 27ss-tail-DNA, suggesting that the A3G activity for this substrate should be very low. However, we did not find a dramatic change in the large oligomer populations for the 42ss-tail-DNA compared with the 69 nt substrates (Figs. 3 and S4), whereas (5) predicted almost a 3-fold drop in deaminase activity. Note that the sequences of our DNA substrates were very close to those in (5). Therefore, a correlation between A3G deaminase activity and the protein oligomeric state apparently exists, however no clear consensus on its dependence can be made at the current time.

This nanoscale AFM analysis of A3G-ssDNA complexes was possible due to the use of the hybrid-DNA methodology and recombinant holoenzyme purified from human HEK293 cells (20, 40). The use of dsDNA segments as molecular rulers allowed us to unambiguously identify specific complexes in the AFM images. In this study, we designed various types of hybrid DNA substrates, enabling us to test a number of hypotheses regarding the A3G-ssDNA interaction. This approach can be applied to answer additional questions on the role(s) of both ssDNA and RNA polynucleotides in the A3G oligomerization and deoligomerization processes.

# **Supplementary Material**

Refer to Web version on PubMed Central for supplementary material.

# **Acknowledgments**

#### **Funding**

The work was supported by grants from National Institutes of Health (P01-GM091743 and R01-GM096039), U.S. Department of Energy Grant DE-FG02-08ER64579, National Science Foundation (EPS – 1004094) and the Nebraska Research Initiative.

We thank P. Beal, M. Kotler, H. Matsuo, J. Mueller and C. Schiffer for critical review of the data and Lyubchenko lab members for helpful discussions.

# **Abbreviations**

A3G APOBEC3G

**AFM** atomic force microscopy **APS** 1-(3-aminopropyl) silatrane

HS-AFM high speed-AFM ssDNA single-stranded DNA

#### References

- 1. Albin JS, Harris RS. Interactions of host APOBEC3 restriction factors with HIV-1 in vivo: implications for therapeutics. Expert Rev Mol Med. 2010; 12:e4. [PubMed: 20096141]
- 2. Malim MH. APOBEC proteins and intrinsic resistance to HIV-1 infection. Philos Trans R Soc Lond B Biol Sci. 2009; 364:675–687. [PubMed: 19038776]

3. Hultquist JF, Lengyel JA, Refsland EW, LaRue RS, Lackey L, Brown WL, Harris RS. Human and rhesus APOBEC3D, APOBEC3F, APOBEC3G, and APOBEC3H demonstrate a conserved capacity to restrict Vif-deficient HIV-1. J Virol. 2011; 85:11220–11234. [PubMed: 21835787]

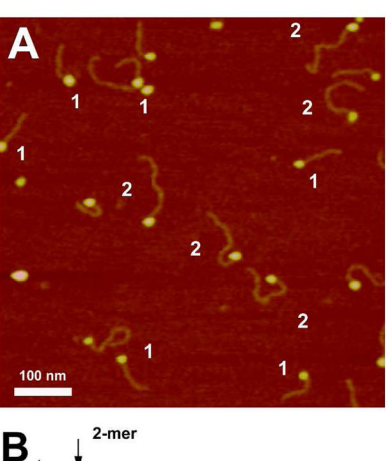
- 4. Huthoff H, Autore F, Gallois-Montbrun S, Fraternali F, Malim MH. RNA-dependent oligomerization of APOBEC3G is required for restriction of HIV-1. PLoS Pathog. 2009; 5:e1000330. [PubMed: 19266078]
- Chelico L, Prochnow C, Erie DA, Chen XS, Goodman MF. Structural model for deoxycytidine deamination mechanisms of the HIV-1 inactivation enzyme APOBEC3G. J Biol Chem. 2010; 285:16195–16205. [PubMed: 20212048]
- Feng Y, Chelico L. Intensity of deoxycytidine deamination of HIV-1 proviral DNA by the retroviral restriction factor APOBEC3G is mediated by the noncatalytic domain. J Biol Chem. 2011; 286:11415–11426. [PubMed: 21300806]
- Chen KM, Harjes E, Gross PJ, Fahmy A, Lu Y, Shindo K, Harris RS, Matsuo H. Structure of the DNA deaminase domain of the HIV-1 restriction factor APOBEC3G. Nature. 2008; 452:116–119. [PubMed: 18288108]
- 8. Holden LG, Prochnow C, Chang YP, Bransteitter R, Chelico L, Sen U, Stevens RC, Goodman MF, Chen XS. Crystal structure of the anti-viral APOBEC3G catalytic domain and functional implications. Nature. 2008; 456:121–124. [PubMed: 18849968]
- Harjes E, Gross PJ, Chen KM, Lu Y, Shindo K, Nowarski R, Gross JD, Kotler M, Harris RS, Matsuo H. An extended structure of the APOBEC3G catalytic domain suggests a unique holoenzyme model. J Mol Biol. 2009; 389:819–832. [PubMed: 19389408]
- Shandilya SM, Nalam MN, Nalivaika EA, Gross PJ, Valesano JC, Shindo K, Li M, Munson M, Royer WE, Harjes E, Kono T, Matsuo H, Harris RS, Somasundaran M, Schiffer CA. Crystal structure of the APOBEC3G catalytic domain reveals potential oligomerization interfaces. Structure. 2010; 18:28–38. [PubMed: 20152150]
- 11. Autore F, Bergeron JR, Malim MH, Fraternali F, Huthoff H. Rationalisation of the differences between APOBEC3G structures from crystallography and NMR studies by molecular dynamics simulations. PLoS One. 2010; 5:e11515. [PubMed: 20635000]
- 12. Li M, Shandilya SM, Carpenter MA, Rathore A, Brown WL, Perkins AL, Harki DA, Solberg J, Hook DJ, Pandey KK, Parniak MA, Johnson JR, Krogan NJ, Somasundaran M, Ali A, Schiffer CA, Harris RS. First-in-class small molecule inhibitors of the single-strand DNA cytosine deaminase APOBEC3G. ACS Chem Biol. 2012; 7:506–517. [PubMed: 22181350]
- 13. Navarro F, Bollman B, Chen H, Konig R, Yu Q, Chiles K, Landau NR. Complementary function of the two catalytic domains of APOBEC3G. Virology. 2005; 333:374–386. [PubMed: 15721369]
- Hache G, Liddament MT, Harris RS. The retroviral hypermutation specificity of APOBEC3F and APOBEC3G is governed by the C-terminal DNA cytosine deaminase domain. J Biol Chem. 2005; 280:10920–10924. [PubMed: 15647250]
- Schumacher AJ, Hache G, Macduff DA, Brown WL, Harris RS. The DNA deaminase activity of human APOBEC3G is required for Ty1, MusD, and human immunodeficiency virus type 1 restriction. J Virol. 2008; 82:2652–2660. [PubMed: 18184715]
- 16. Chelico L, Pham P, Calabrese P, Goodman MF. APOBEC3G DNA deaminase acts processively 3' '--> 5' on single-stranded DNA. Nat Struct Mol Biol. 2006; 13:392–399. [PubMed: 16622407]
- 17. Shindo K, Takaori-Kondo A, Kobayashi M, Abudu A, Fukunaga K, Uchiyama T. The enzymatic activity of CEM15/Apobec-3G is essential for the regulation of the infectivity of HIV-1 virion but not a sole determinant of its antiviral activity. J Biol Chem. 2003; 278:44412–44416. [PubMed: 12970355]
- Chelico L, Sacho EJ, Erie DA, Goodman MF. A model for oligomeric regulation of APOBEC3G cytosine deaminase-dependent restriction of HIV. J Biol Chem. 2008; 283:13780–13791. [PubMed: 18362149]
- McDougall WM, Smith HC. Direct evidence that RNA inhibits APOBEC3G ssDNA cytidine deaminase activity. Biochem Biophys Res Commun. 2011; 412:612–617. [PubMed: 21856286]
- Shlyakhtenko LS, Lushnikov AY, Li M, Lackey L, Harris RS, Lyubchenko YL. Atomic force microscopy studies provide direct evidence for dimerization of the HIV restriction factor APOBEC3G. J Biol Chem. 2011; 286:3387–3395. [PubMed: 21123176]

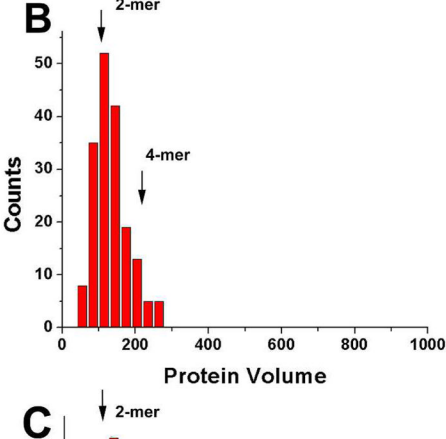
21. Roberts SA, Sterling J, Thompson C, Harris S, Mav D, Shah R, Klimczak LJ, Kryukov GV, Malc E, Mieczkowski PA, Resnick MA, Gordenin DA. Clustered mutations in yeast and in human cancers can arise from damaged long single-strand DNA regions. Mol Cell. 2012; 46:424–435. [PubMed: 22607975]

- 22. Nowarski R, Wilner OI, Cheshin O, Shahar OD, Kenig E, Baraz L, Britan-Rosich E, Nagler A, Harris RS, Goldberg M, Willner I, Kotler M. APOBEC3G enhances lymphoma cell radioresistance by promoting cytidine deaminase-dependent DNA repair. Blood. 2012
- 23. Nik-Zainal S, Alexandrov LB, Wedge DC, Van Loo P, Greenman CD, Raine K, Jones D, Hinton J, Marshall J, Stebbings LA, Menzies A, Martin S, Leung K, Chen L, Leroy C, Ramakrishna M, Rance R, Lau KW, Mudie LJ, Varela I, McBride DJ, Bignell GR, Cooke SL, Shlien A, Gamble J, Whitmore I, Maddison M, Tarpey PS, Davies HR, Papaemmanuil E, Stephens PJ, McLaren S, Butler AP, Teague JW, Jonsson G, Garber JE, Silver D, Miron P, Fatima A, Boyault S, Langerod A, Tutt A, Martens JW, Aparicio SA, Borg A, Salomon AV, Thomas G, Borresen-Dale AL, Richardson AL, Neuberger MS, Futreal PA, Campbell PJ, Stratton MR. Mutational Processes Molding the Genomes of 21 Breast Cancers. Cell. 2012; 149:979–993. [PubMed: 22608084]
- Shlyakhtenko LS, Lushnikov AY, Miyagi A, Lyubchenko YL. Specificity of binding of singlestranded DNA-binding protein to its target. Biochemistry. 2012; 51:1500–1509. [PubMed: 22304461]
- 25. Lyubchenko YL, Shlyakhtenko LS. AFM for analysis of structure and dynamics of DNA and protein-DNA complexes. Methods. 2009; 47:206–213. [PubMed: 18835446]
- Uchihashi T, Ando T. High-speed atomic force microscopy and biomolecular processes. Methods Mol Biol. 2011; 736:285–300. [PubMed: 21660734]
- Shlyakhtenko LS, Gilmore J, Kriatchko AN, Kumar S, Swanson PC, Lyubchenko YL. Molecular mechanism underlying RAG1/RAG2 synaptic complex formation. J Biol Chem. 2009; 284:20956– 20965. [PubMed: 19502597]
- 28. Shlyakhtenko LS, Lushnikov AY, Lyubchenko YL. Dynamics of nucleosomes revealed by time-lapse atomic force microscopy. Biochemistry. 2009; 48:7842–7848. [PubMed: 19618963]
- 29. Yamamoto D, Uchihashi T, Kodera N, Yamashita H, Nishikori S, Ogura T, Shibata M, Ando T. High-speed atomic force microscopy techniques for observing dynamic biomolecular processes. Methods Enzymol. 2010; 475:541–564. [PubMed: 20627170]
- Ando T. High-speed atomic force microscopy coming of age. Nanotechnology. 2012; 23:062001.
   [PubMed: 22248867]
- 31. Lyubchenko YL, Shlyakhtenko LS, Ando T. Imaging of nucleic acids with atomic force microscopy. Methods. 2011; 54:274–283. [PubMed: 21310240]
- 32. Miyagi A, Ando T, Lyubchenko YL. Dynamics of nucleosomes assessed with time-lapse high-speed atomic force microscopy. Biochemistry. 2011; 50:7901–7908. [PubMed: 21846149]
- 33. Chelico L, Pham P, Goodman MF. Mechanisms of APOBEC3G-catalyzed processive deamination of deoxycytidine on single-stranded DNA. Nat Struct Mol Biol. 2009; 16:454–455. author reply 455–456. [PubMed: 19421154]
- 34. Iwatani Y, Takeuchi H, Strebel K, Levin JG. Biochemical activities of highly purified, catalytically active human APOBEC3G: correlation with antiviral effect. J Virol. 2006; 80:5992–6002. [PubMed: 16731938]
- 35. Chelico L, Pham P, Calabrese P, Goodman MF. APOBEC3G DNA deaminase acts processively 3'--> 5' on single-stranded DNA. Nat Struct Mol Biol. 2006; 13:392–399. [PubMed: 16622407]
- 36. Nowarski R, Britan-Rosich E, Shiloach T, Kotler M. Hypermutation by intersegmental transfer of APOBEC3G cytidine deaminase. Nat Struct Mol Biol. 2008; 15:1059–1066. [PubMed: 18820687]
- 37. Harris RS, Bishop KN, Sheehy AM, Craig HM, Petersen-Mahrt SK, Watt IN, Neuberger MS, Malim MH. DNA deamination mediates innate immunity to retroviral infection. Cell. 2003; 113:803–809. [PubMed: 12809610]
- 38. Suzuki Y, Gilmore JL, Yoshimura SH, Henderson RM, Lyubchenko YL, Takeyasu K. Visual analysis of concerted cleavage by type IIF restriction enzyme SfiI in subsecond time region. Biophys J. 2011; 101:2992–2998. [PubMed: 22208198]

39. Senavirathne G, Jaszczur M, Auerbach PA, Upton TG, Chelico L, Goodman MF, Rueda D. Single-stranded DNA scanning and deamination by APOBEC3G cytidine deaminase at single molecule resolution. J Biol Chem. 2012; 287:15826–15835. [PubMed: 22362763]

40. Nowarski R, Britan-Rosich E, Shiloach T, Kotler M. Hypermutation by intersegmental transfer of APOBEC3G cytidine deaminase. Nat Struct Mol Biol. 2008; 15:1059–1066. [PubMed: 18820687]





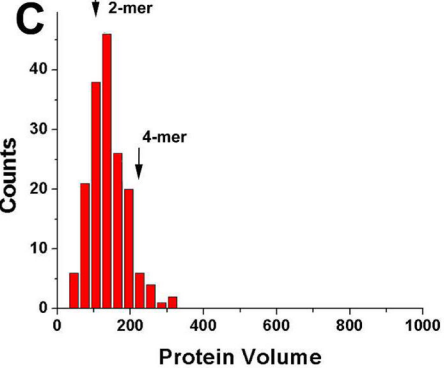


**Figure 1.**AFM image (A) and the volume distribution histogram in (B) and (C) corresponding to a (B) 5'-69ss tail-DNA (N=180, yield of the complexes) and a (C)-3'-69ss tail-DNA (N=170, yield of the complexes). In panel (A), "1" represents complexes with a 5'-69ss tail-DNA (231 bp duplex), while "2" shows 3'-69ss tail-DNA (436 bp duplex). Arrows in (B) and (C) indicated positions of dimers (2-mers) and tetramers (4-mers).

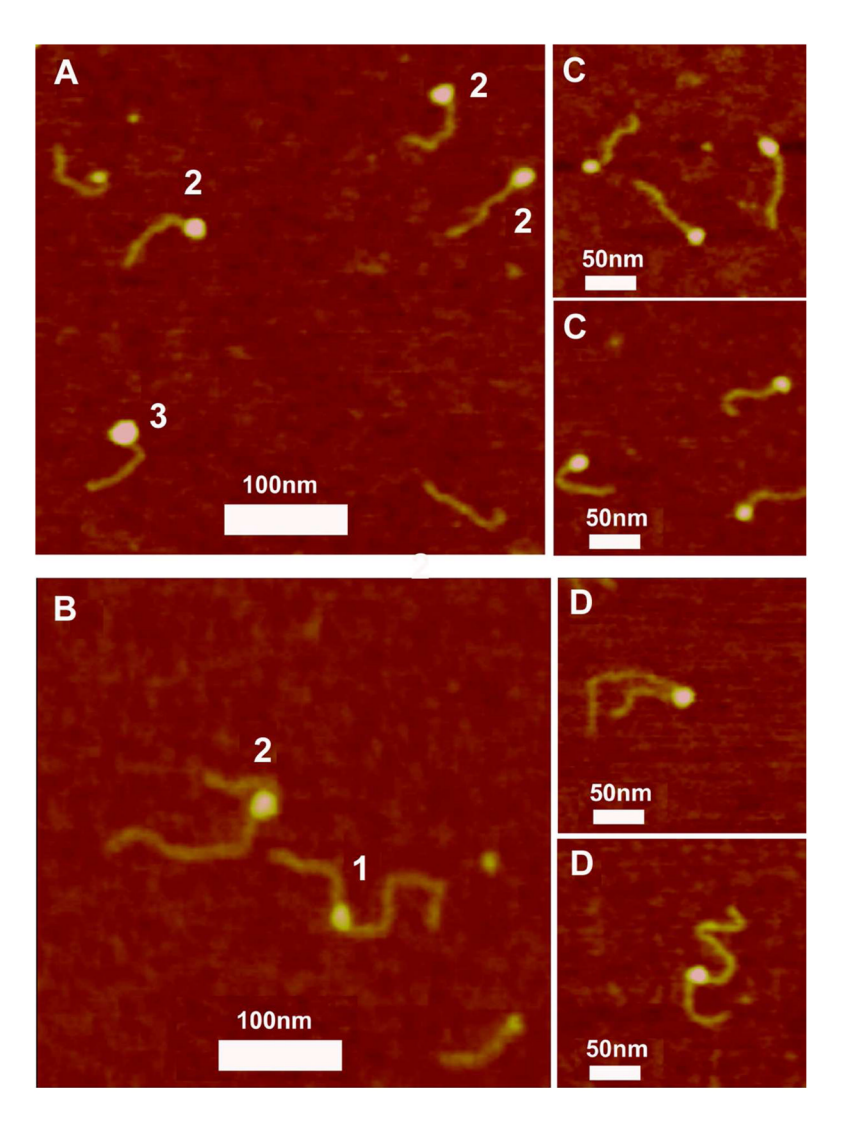


**Figure 2.**AFM images of complexes of A3G with tail-DNA and gap-DNA substrates containing a 69 nt ssDNA. (A). AFM image of the A3G complex with 69ss tail-DNA. Molecule labels: 2-dimers, 3- trimers. (B). AFM image of the A3G complex with 69ss gap-DNA. Molecule labels: 1-monomer, 2- dimer. (C). The gallery of AFM images of complexes of A3G with the 69ss tail-DNA. (D). The gallery of AFM images of complexes of A3G with the 69ss gap-DNA.

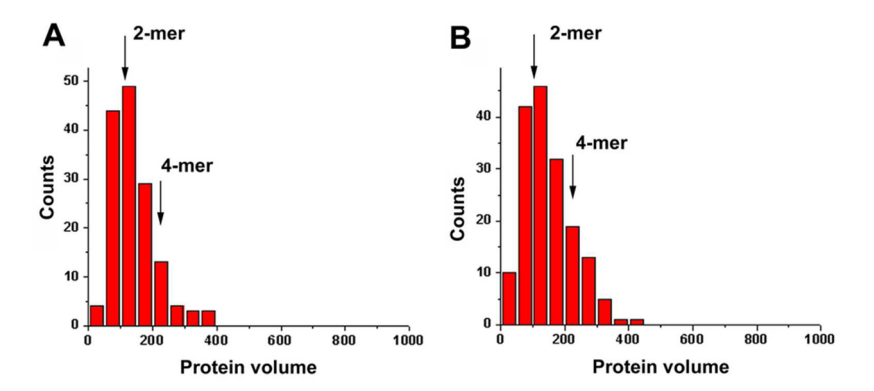


**Figure 3.** Histograms for the A3G volume measurements (A) A3G in complexes with the 69ss-tail-DNA (N=152). (B) A3G in complexes with the 69ss-gap-DNA (N=170). The arrows show the positions of the A3G dimers and tetramers.

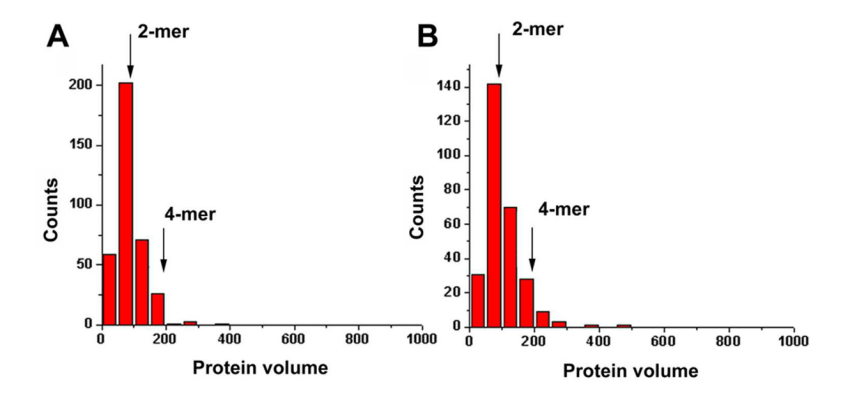
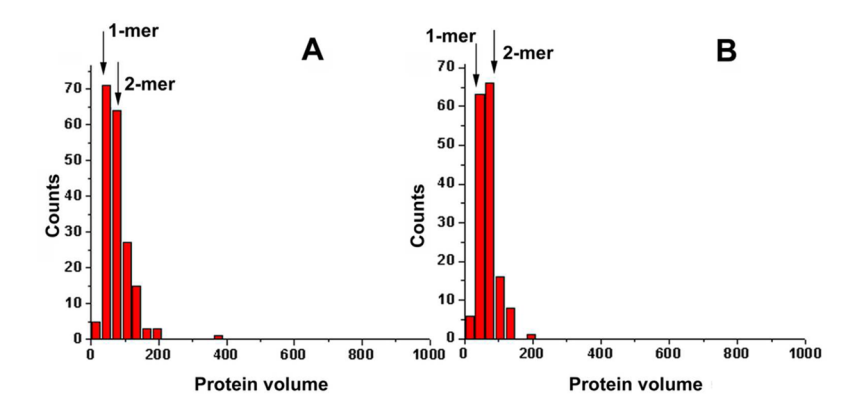
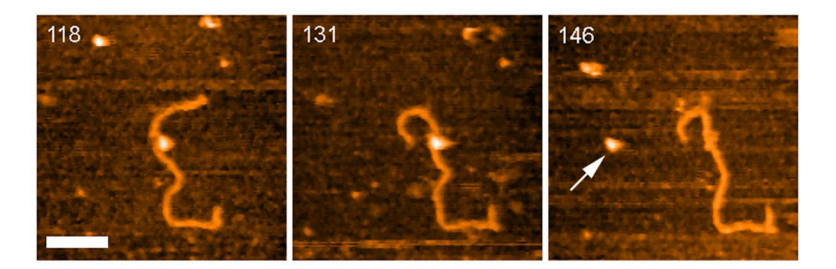


Figure 4. Histograms for the A3G volume measurements in complexes with the 27ss- tail-DNA (A) 3'- tail-DNA (N=362), and (B) 5'-tail- DNA (N=284). The arrows point to the A3G dimers and tetramers. The yields of the complexes for 5'-tail DNA and 3'-tail DNA are 34% and 35%, respectively.



**Figure 5.** Histograms for the A3G volume measurements in complexes with the 18 nt tail-DNA. (A) 3'- tail-DNA (N=150), and (B) 5'-tail- DNA (N=160). The arrows show the positions of the A3G monomers and dimers.



**Figure 6.** High speed AFM images demonstrating A3G dissociation. Three frames from Movie S1 (SI) illustrate one-step dissociation of A3G dimer (arrow indicates position of dissociated A3G). Bar size 50nm, each frame 720ms.

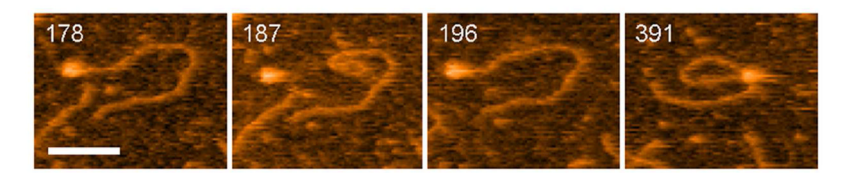


**Figure 7.**Selected frames demonstrating one-step dissociation followed by the complex formation of the A3G dimer with 27nt tail-DNA (Movie 2 in Supporting Information). Bar size 30nm. Each frame 720 ms

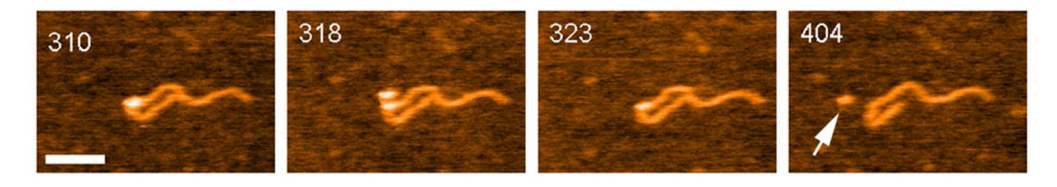


**Figure 8.**Two step A3G dissociation from the gap-DNA substrate (Movie S3 in SI). Bar size 50 nm. Each frame 720 ms. Arrow indicates position of dissociated A3G.

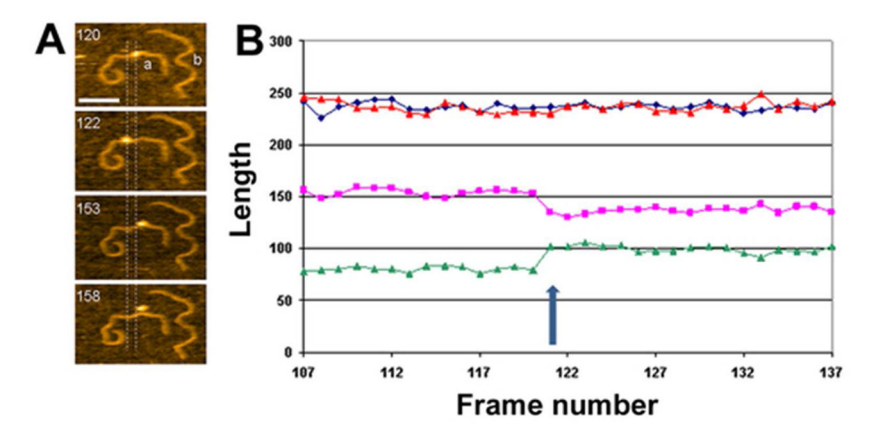


Figure 9.
Sliding of A3G. (A) Selected frames for A3G-gap-DNA complex (a) and gap-DNA (b) (Movie 4 in Supporting Information). Bar size 50nm. Each frame 720 msec. Vertical dotted lines show the distance between ends of DNA arms and the center of the protein. (B) The DNA contour length in the complex with A3G (a-blue) and without protein (b-red). The length for the left (purple) and right (green) DNA arms measured from the end to the center of the protein. Arrow points to the protein translocation event.

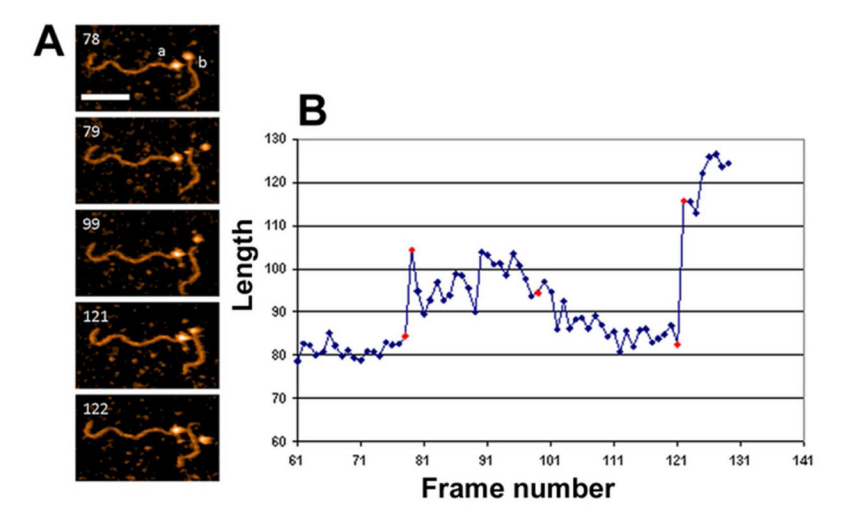


Figure 10.
The protein dynamics for the end-bound complex (Movie 5 in Supporting Information). (A) Selected frames for A3G-tail-DNA complexes. Bar size 50nm. Each frame 720 ms. (B) The distance measured between the distant end of the DNA (molecule b) and the center of the protein for each frame. Red points on the graph correspond to the frames in (A).